EAST EUROPEAN JOURNAL OF PHYSICS. **1.** 154-161 (2023)
DOI:10.26565/2312-4334-2023-1-19 ISSN 2312-4334

SYNTHESIS OF SnS/SnO NANOSTRUCTURE MATERIAL FOR PHOTOVOLTAIC APPLICATION†

Egwunyenga N. Josephine[a,b], Okunzuwa S. Ikponmwosa[b], Imosobomeh L. Ikhioya[c]*
[a]*Department of Science Laboratory Technology, Delta State Polytechnic, Ogwashi-Uku, Nigeria*
[b]*Department of Physics, University of Benin, Benin*
[c]*Department of Physics and Astronomy, University of Nigeria, Nsukka, 410001, Enugu State, Nigeria*
**Corresponding Author e-mail: imosobomeh.ikhioya@unn.edu.ng, nkeopene@gmail.com*
Received December 9, 2022; revised January 3, 2023; accepted January 16, 2023

Research Highlights:

- Successfully synthesized SnS/SnO nanostructured material using successors ionic layer absorption and reaction (SILAR) technique.
- Granular nanocrystals were visible in the materials, and they were strewn unevenly and randomly throughout the glass surface.
- It was found that the sample processed at room temperature had the largest energy band gap.
- The transmittance in the visible area of the spectrum was stable and SnS/SnO was at its maximum in the UV region

In this research, the SILAR method was used to synthesize environmentally-friendly SnS/SnO material for photovoltaic application, where 0.1 M of tin (II) chloride dihydrate ($SnCl_2.2H_2O$) was used to create the cationic precursor solution, and 0.01 M of thioacetamide (C_2H_5NS) was used to create the anionic precursor solution. The X-ray diffraction patterns of SnS/SnO material deposited on glass substrate at various deposition temperatures recorded a major peak at 45°C at 2 theta of 31.8997°, which corresponds to the face-centered cubic crystal structure (FCC). Diffraction peaks are visible in the pattern at planes 111, 200, 210, 211, and 300, which correspond to angles of 26.58°, 31.89°, 39.61°, 44.18°, and 54.85°, respectively. It was discovered that the crystallite/grain size and the lattice parameters decrease as the temperature of the deposition material rises. Granular nanocrystals were visible in the materials, and they were strewn unevenly and randomly throughout the glass surface. The spectra of the absorbance demonstrate that as light radiation passed through SnS/SnO films, it absorbed radiation as the wavelength increased from the UV region to the ultraviolet region of the spectra. It was discovered that the precursor temperature influences the material's absorbance; as the temperature rises, the absorbance decreases, making SnS/SnO an excellent material for photovoltaic systems. The transmittance in the visible area of the spectrum was stable and SnS/SnO was at its maximum in the UV region, it increased as the wavelength increased in the NIR region. It was found that the sample processed at room temperature had the largest energy band gap. SnS/SnO reveals an increase in thickness from 114.42 – 116.54 nm which resulted in a downturn in the resistivity of the deposited film from 9.040×10^{9} – 6.455×10^{9} (Ω·cm) while the conductivity of the deposited material increased from 1.106×10^{-10} – 1.549×10^{-10} $(\Omega\cdot cm)^{-1}$.

Keywords: *Tin sulphide; Nanocrystals; Nanostructure; EDX; XRD; SEM*
PACS: 72.80.Ey, 78.67.Bf, 62.23.St, 83.85.Hf, 78.70.Dm, 87.64.Dz

1. INTRODUCTION

Recently, there has been a lot of interest in the possible applications of semiconducting metal chalcogenide thin films in solid-state devices, such as photovoltaic, photoelectrochemical, photoconductive cells, solar cells, sensors, etc. The most interest has been shown in thin sulphide, a semiconducting metal chalcogenide with a high optical absorption coefficient and photoelectric conversion efficiency. An IV-VI semiconductor built of cheap, plentiful, and non-toxic SnS. It is possible to produce ecologically acceptable semiconductor materials for solar energy applications, such as tin sulphide and tin oxide, using the SILAR method. SnO_2 and SnS are important conversion materials because of their widespread natural occurrence, high theoretical gravimetric capacity, and environmental friendliness [1]. As a prospective window/buffer layer material for heterojunction solar cells, SnO_2 is considered one of the more recently approved transparent conducting oxides. However, it's an n-type semiconductor with a broad energy band gap of 3.8 eV and a higher molarity of free electrons than holes.

The SnS, on the other hand, is regarded as a more advantageous absorption layer material due to its high absorption coefficient, the p-type semiconductor band gap of 1.3 eV, and significantly higher hole concentration [2]. As a result, at the junction between the two semiconductors, holes diffuse from the SnS to the SnO2, as opposed to the SnO_2 in the case of the latter. Due to its high optical transparency (T>85% in the visible region), low electrical resistance, and good thermal resistance, tin oxide has primarily been used in a large number of optoelectronic devices, such as light-emitting diodes, buffer layer materials in solar cells, transparent filled effect transistors, etc. [3]. Tin oxide (SnO_2) is among the most important n-type semiconductors. The charge carriers annihilate at the intersection of these two diffusion modes, producing an internal electric field that accelerates the active movement of charges and ions and, as a result, results in high-rate capability [4]. SnS/SnO_2 heterostructures have a wide range of possible applications, from high-speed electronics to optoelectronics devices, because of their special interface features [5-7]. Because of the multiple heterojunction structures, the SnS/SnO_2 heterostructure exhibits significantly improved photocatalytic and photoelectrochemical performances. In addition, because SnS is more reversible than comparable oxides, it has a higher initial coulombic efficiency and reversible capacity [8-10].

† ***Cite as:*** E.N. Josephine, O.S. Ikponmwosa, and I.L. Ikhioya, East Eur. J. Phys. **1**, 154 (2023), https://doi.org/10.26565/2312-4334-2023-1-19

Sugiyama et al., who created a typical SnS-based solar cell with a glass/SnO_2/SnS/CdS/ZnO configuration, claim that they measured band discontinuities at SnO_2/SnS heterointerfaces using X-ray photoelectron spectroscopy and found that SnO_2/SnS interfaces produced evaluated valence band offsets of about 3.5 eV [11]. El-Etre and Red (2010) [12] created a nanocrystalline SnO_2 thin film using cathodic electrodeposition-anodic oxidation and then used X-ray diffraction, SEM, UV-visible absorption, and nitrogen adsorption-desorption by BET technique to determine the structure of the film. The final film has a grain size of 24 nm and a surface area of 137.9 m^2/g. In dye-sensitized solar cells, the produced SnO_2 thin film can therefore be used as an electrode. Tin oxide (SnO_2), one of many metal oxides, has drawn a lot of attention as a viable candidate material due to its myriad uses. SnO_2 is widely utilized for a variety of high-tech applications, including dye-sensitized solar cells, gas sensors, photocatalysts, lithium-ion batteries, and supercapacitors, to mention a few [13]. These applications include optical and electrical qualities, high chemical stability, and theoretical capacity.

The films can be created using several techniques, such as spray pyrolysis, electrode placement, chemical bath deposition (CBD), vacuum evaporation, SILAR, etc. SILAR is the most straightforward, affordable, and quickly implemented method available [14-17]. Broad surfaces can be covered with thin films using SILAR, and the thickness can be changed by adjusting the number of dippings.

In this research, the successor's ionic layer absorption and reaction (SILAR) technique were used to synthesize environmentally-friendly SnS/SnO material for photovoltaic application, were 0.1 M of tin (II) chloride dihydrate ($SnCl_2{\cdot}2H_2O$) was used to create the cationic precursor solution, and 0.01 M of thioacetamide (C_2H_5NS) was used to create the anionic precursor solution. The film will be characterized for their Phase identification by X-ray diffraction and scanning electron microscope (SEM) model A-VPSE G3 was used to determine the chemical compositions of the thin films produced in this work.

2. EXPERIMENTAL PROCEDURE

The following precursors were employed in the deposition of SnS/SnO: 0.1 M of tin (II) chloride dihydrate ($SnCl_2.2H_2O$) was used to create the cationic precursor solution, and 0.01 M of thioacetamide (C_2H_5NS) was used to create the anionic precursor solution. Four sets of 50 ml beakers containing tin (II) chloride dihydrate ($SnCl_2{\cdot}2H_2O$) solution. Distilled water, and Thioacetamide (C_2H_5NS)/potassium hydroxide (KOH) solution. A well-cleaned glass substrate that had been washed with acetone, distilled water, and acid was submerged in a cationic precursor solution of tin (II) chloride dihydrate ($SnCl_2{\cdot}2H_2O$) for 10 seconds to allow tin ions to adhere to the surface of the substrate. To get rid of the loosely attached Sn^{2+} ions, the substrate was washed in distilled water for 5 seconds. The substrate was then submerged in the Thioacetamide (C_2H_5NS)/potassium hydroxide (KOH) anionic precursor solution for 10 seconds to create a layer of SnS/SnO materials. One SILAR cycle of SnS deposition was finished by rinsing the substrate once more in distilled water for 5 s to remove the unreached species. Such cycles were repeated for various variations at various temperatures. The precursor pH was kept constant at 7.0 while all other parameters, including the deposition temperature, varied between 50ºC, 55ºC, 60ºC, and 65ºC during the synthesis. Tin sulphide (SnS) was next deposited on the developed SnO films to create SnS/SnO superlattice films, and the process was repeated for a different parameter for characterization. Tin oxide (SnO) was initially coated on the glass substrate dry in the oven for 30 minutes.

2.1. Characterization Techniques

The characterization of the deposited films was ascertained using some currently in-use techniques. Knowing the chemical composition, crystal structure, crystallite size, surface morphology, band gap energy, optical absorption, transmittance, and absorbance of the formed film is possible thanks to characterization. Phase identification of the films by X-ray diffraction was used to determine the chemical compositions of the thin films produced in this work using a scanning electron microscope (SEM) model A-VPSE G3 with an acceleration voltage of 20 kV and a magnification range of 200x to 1000x, the morphology and size of the prepared particles were investigated. The optical characteristics of the films deposited were examined for their absorbance and transmittance at normal incidence by using a UV-visible spectrophotometer, model number 756S.

3. RESULTS AND DISCUSSIONS

Figure 1 displays the X-ray diffraction patterns of SnS/SnO material deposited on a glass substrate at various temperatures. The major peak was discovered at 45ºC at 2 theta of 31.8997º, which corresponds to the face-centered cubic crystal structure (FCC). SnS/SnO was recognized as the orientations along the (200) plane and the (300), respectively. It was stated that the lattice constant was $\alpha = 5.8028$ Å. Several peaks were found to support the usage of SnS/SnO material as a hole transport material in solar cells and photovoltaic systems. The SILAR method was used to deposit this material. The Debye-Scherrer equation was used to calculate the average crystallite sizes based on the diffraction peaks' full width at half maximums (FWHM). The polycrystalline nature of the films was revealed by the XRD pattern. Diffraction peaks are visible in the pattern at planes 111, 200, 210, 211, and 300, which correspond to angles of 26.58°, 31.89°, 39.61°, 44.18°, and 54.85°, respectively. The unindexed peaks could have been brought on by the glass substrates used for the deposition. Table 1 displays the calculated structural characteristics of the material. It was discovered that the crystallite/grain size and the lattice parameters decrease as the temperature of the deposition material rises. This size reduction would increase the crystallinity of the deposited films and increase the efficiency of photon absorption.

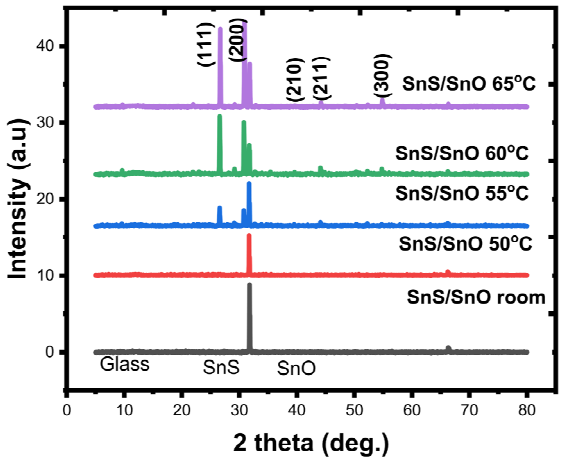

Figure 1. XRD pattern of SnS/SnO material

Table 1. Structural values for the SnS/SnO

Films	2θ (degree)	Spacing d(Å)	Lattice constant (Å)	FWH, β	Hkl	Crystallite Size, D (nm)	Dislocation density, δ m^2
SnS/SnO room	26.5815	3.3502	5.8028	0.1851	111	0.7694	5.1218
SnS/SnO 50°C	31.8997	2.8028	5.6056	0.2095	200	0.6880	6.4151
SnS/SnO 55°C	39.6196	2.2726	5.5453	0.1480	210	0.6957	6.0633
SnS/SnO 60°C	44.1829	2.0479	4.5793	0.2258	211	0.7626	6.8539
SnS/SnO 65°C	54.8536	1.6721	4.0958	0.2249	300	0.7543	6.2663

3.1. SEM Micrograph of SnS/SnO Material

The surface micrograph of SnS/SnO material deposited at various precursor temperatures (45°C-65°C) is shown in Figure 2.

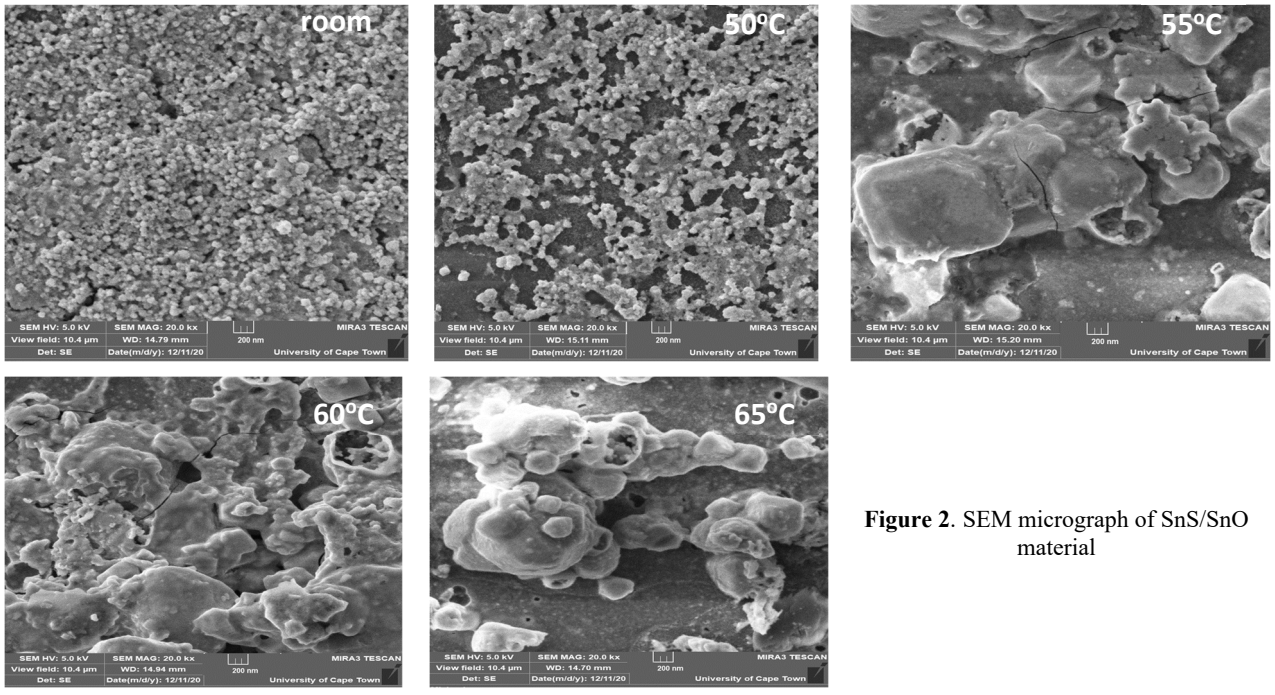

Figure 2. SEM micrograph of SnS/SnO material

All of the deposited materials' surface morphological images were scanned at a magnification of 200 nm. Granular nanocrystals were visible in the materials, and they were strewn unevenly and randomly throughout the glass surface. In contrast to SnS/SnO deposited at 50°C, which has a similar image but shows the particle is scattered on the glass surface, the SnS/SnO image at room temperature shows sand-like particles well packed together without pinholes, while the material is deposited between 55 and 65 degrees Celsius, the nano grain is larger than when it is placed at 50 degrees. The material left behind demonstrates how the growth of big grains led to the agglomeration of the particles. The films' increasing grain sizes demonstrate that as the precursor temperature rises, the size of the crystallites also grows, providing more room for light absorption and trapping following penetration. This property makes the deposited films potential

photovoltaic materials. The elemental constituents of SnS/SnO material showed in Figure 3. The position of the peaks in a typical EDX spectrum confirms the presence of the fundamental elements, and the peak height helps quantify each element's concentration in the film samples. The material's EDX results show that tin, sulfur, and oxygen are present, with a greater intensity peak for tin and oxygen and proof of sulfur's presence. The constituent elements of the glass substrate used for the deposition were created as a result of the other element on the spectrum.

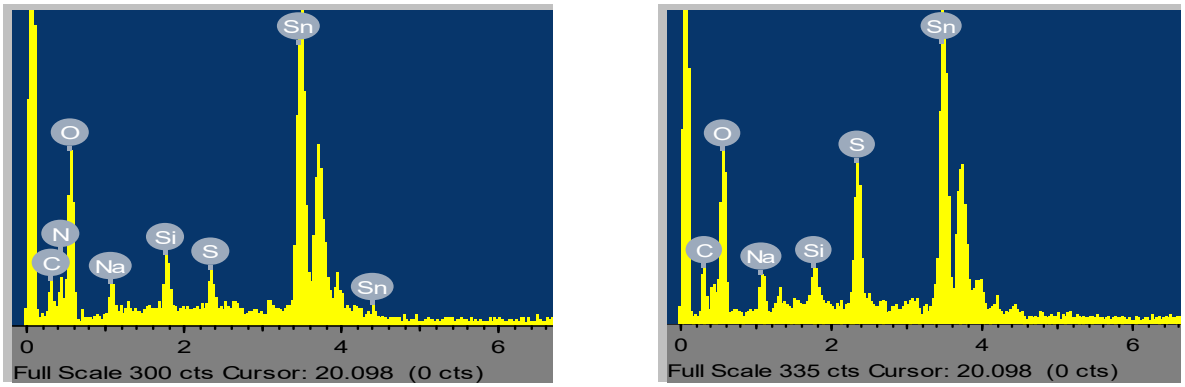

Figure 3. EDX spectra

3.2. The optical study

The SnS/SnO was investigated for their optical examination to determine how quickly it absorbed light. According to Figure 4(“a”), the spectra of the absorbance demonstrate that as light radiation passed through SnS/SnO films, it absorbed radiation as the wavelength increased from the UV region to the ultraviolet region of the spectra. The absorbance also slightly decreased along the NIR infrared region as the wavelength increased.

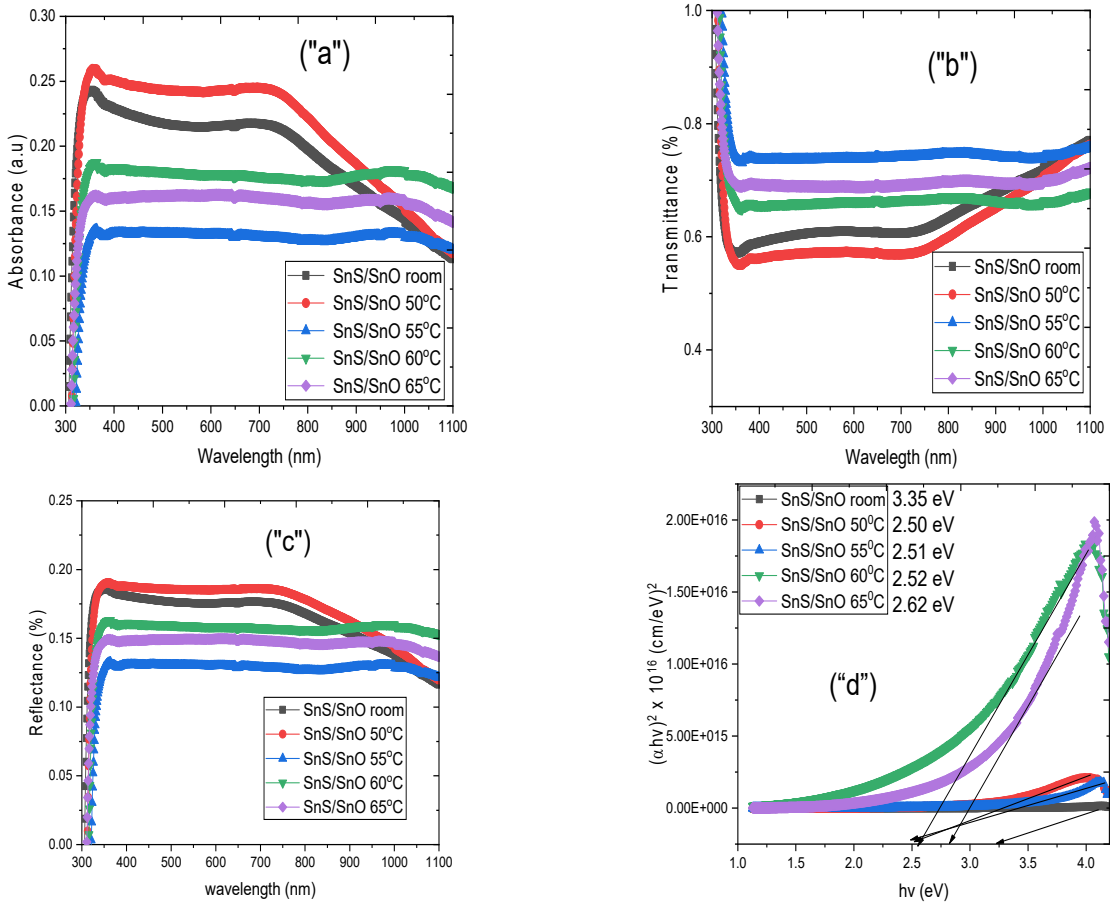

Figure 4. (“a”) absorbance, (“b”) transmittance, (“c”) reflectance, and (“d”) band gap energy

It was discovered that the precursor temperature influences the material's absorbance; as the temperature rises, the absorbance decreases, making SnS/SnO an excellent material for photovoltaic systems. Figure 4(“b”) depicts the SnS/SnO material's transmittance. While the transmittance in the visible area of the spectrum was stable and SnS/SnO was at its maximum in the UV region, it increased as the wavelength increased in the NIR region. The transmittance was also

impacted by temperature, which led to an increase in SnS/SnO transmittance in the UV and ultraviolet parts of the spectrum. From Figure 4("c"), the reflectance decreases as wavelength increases. The reflectance is moderate at the visible region. It also shows that the reflectance reduces, with an increase in the temperature of the precursor. The energy band gap spectra of the deposited SnS/SnO films are depicted in Figure 4 ("d") and were estimated using the Tauc equation: $(\alpha h\upsilon)^{1/n} = \beta(h\upsilon - E_g)$. 3.35 eV is the band gap determined from the film at ambient temperature. It was found that the sample processed at room temperature had the largest energy band gap. 2.50 eV, 2.51 eV, 2.52 eV, and 2.62 eV are the calculated energy band gap values.

The extinction coefficient of the SnS/SnO material is plotted in Figure 5 ("a"). The extinction coefficient gradually rises as the spectra's energy level approaches. It also showed how the precursor temperature affected the films. Using equation 1, the reflectance data were used to estimate the refractive index is shown in Figure 5 ("b")

$$\boldsymbol{n = \frac{1+R}{1-R} + \sqrt{\frac{4R}{(1-R)^2} - K^2}}. \quad (1)$$

The non-linear refractive index pattern suggests a change in the samples' typical dispersion characteristics. This demonstrates how the refractive index is independent of wavelength. Higher deposition temperatures caused the visible part of the electromagnetic spectrum, where it ends at a value of 1.11, to have narrower spectra. The sample that was deposited at 60°C had a wider spectrum, while the sample that was deposited at 65°C was second. The sample deposited at 70°C had a wider spectrum than the sample deposited at 50°C in terms of the sequence. The sample deposited at 55°C has the narrowest spectrum. Electrical transport at high optical frequencies is related to quantitative measurements in Figure 5 ("c") optical conductivity. The optical conductivity spectra of a material are frequently used to describe its response to light. Its dimensions are measured in units per second (S^{-1}), which are equivalent to the frequency in the Gaussian unit. A progressive climb towards higher energy levels is followed by a decrease in the optical conductivity of the SnS/SnO material.

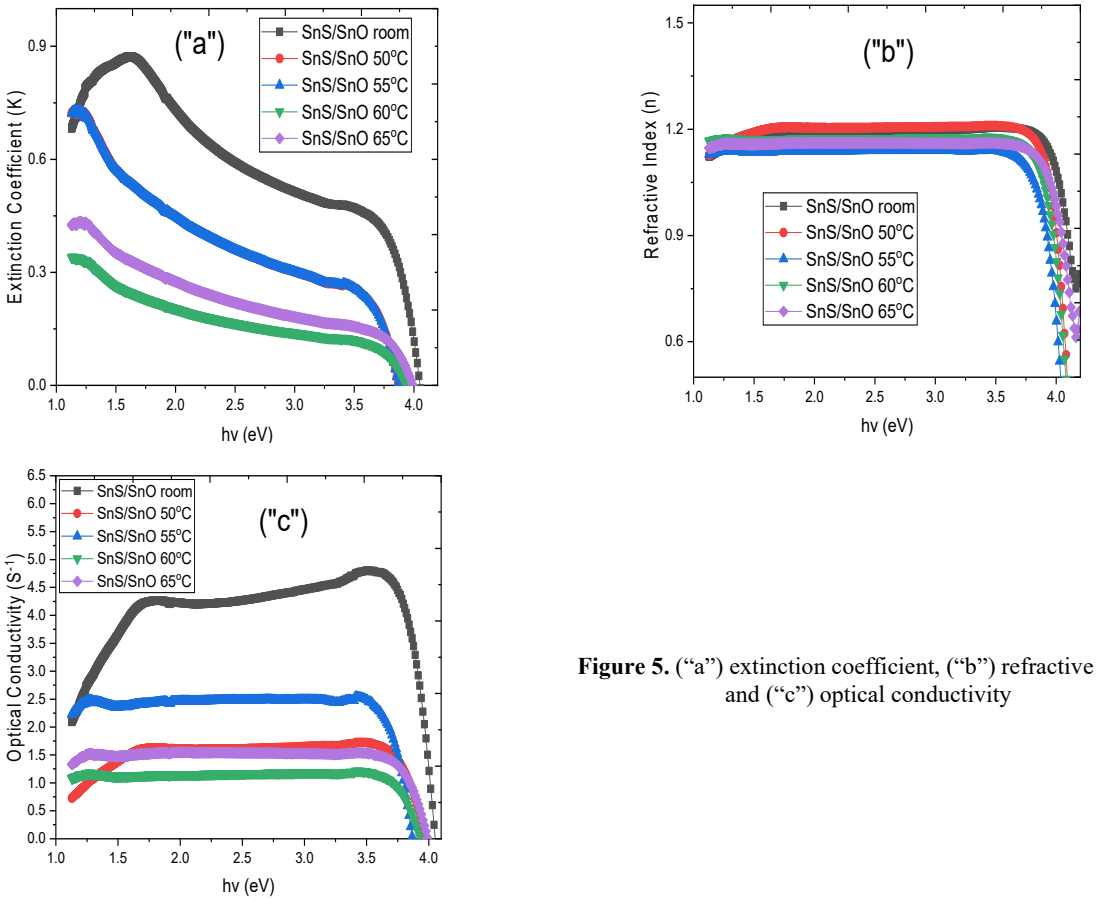

Figure 5. ("a") extinction coefficient, ("b") refractive index, and ("c") optical conductivity

Figures 6 ("a") and ("b") demonstrate the dielectric constant of SnS/SnO; the former indicates energy loss; the latter indicates how effectively dielectric materials store electrical energy. Permittivity in alternating current fields includes both real and fictitious components that, respectively, represent dielectric losses and polarization levels. Furthermore, affected by frequency is the dielectric constant. The spectra of the real and imaginary dielectric constants of the deposited SnS/SnO showed that the real and imaginary dielectric constant values increased with the photon energy of the material. This demonstrates that the deposited materials become helpful for solar systems when their temperature is raised.

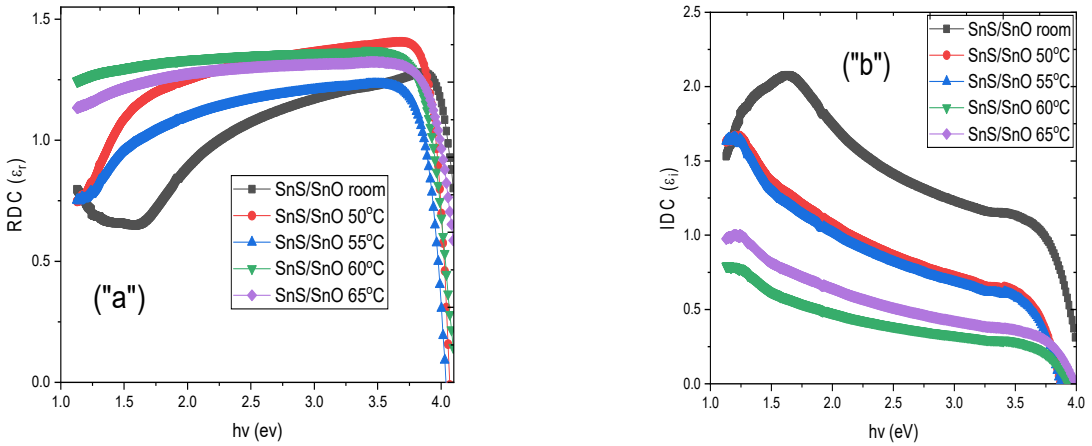

Figure 6. ("a") real, and ("b") imaginary dielectric constant

The material deposited at different temperatures reveals an increase in thickness from 114.42 – 116.54 nm which resulted in a downturn in the resistivity of the deposited film from 9.040×10^{9} – 6.455×10^{9} (Ω.cm) while the conductivity of the deposited material increased from 1.106×10^{-10} - 1.549×10^{-10} $(\Omega\cdot cm)^{-1}$. Figure 7 ("a") and ("b") show the plot of resistivity and conductivity against thickness and precursor temperature, from the plot increase in thickness, resulted in an increase in conductivity and a decrease in resistivity and an increase in precursor temperature beginning about the increase in conductivity and decrease in resistivity. The deposited material will be a good candidate for photovoltaic and solar cell applications.

Table 2. Electrical properties of SnS/SnO

Films	Thickness, t (nm)	Resistivity, **ρ** (Ω.cm)×10^{9}	Conductivity, **σ** (S/m)×10^{-10}
SnS/SnO room	114.42	9.040	1.106
SnS/SnO 50°C	115.32	8.237	1.214
SnS/SnO 55°C	115.42	7.643	1.308
SnS/SnO 60°C	116.33	7.431	1.345
SnS/SnO 65°C	116.54	6.455	1.549

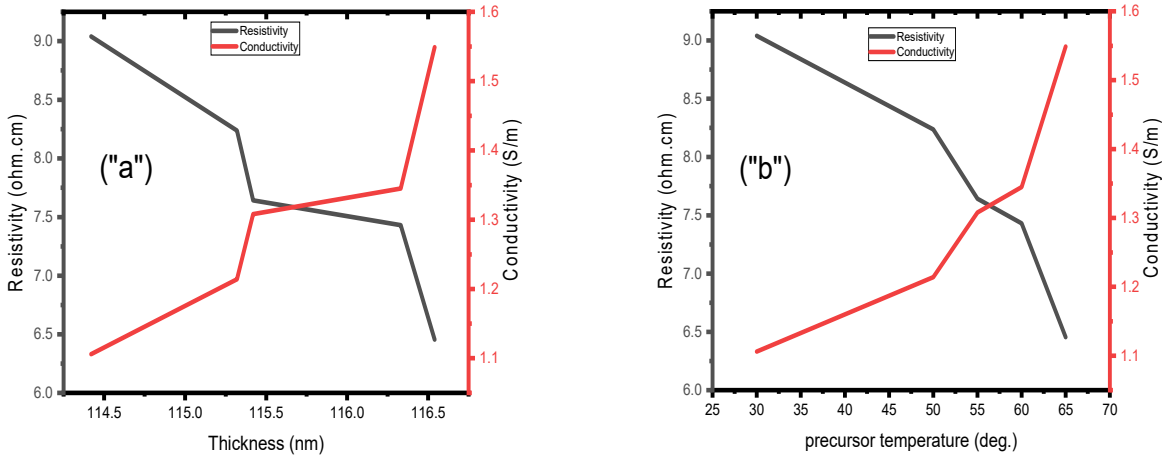

Figure 7. ("a") plot of resistivity and conductivity against thickness and ("b") precursor temperature

4. CONCLUSION

SnS/SnO material has been successfully deposited using the SILAR method. The X-ray diffraction patterns of SnS/SnO material deposited on glass substrate at various deposition temperatures recorded a major peak at 45°C at 2 theta of 31.8997°, which corresponds to the face-centered cubic crystal structure (FCC). SnS/SnO was recognized as the orientations along the (200) plane and the (300), respectively. It was stated that the lattice constant was $\alpha = 5.8028$ Å. Several peaks were found to support the usage of SnS/SnO material as a hole transport material in solar cells and photovoltaic systems. The polycrystalline nature of the films was revealed by the XRD pattern. Diffraction peaks are visible in the pattern at planes 111, 200, 210, 211, and 300, which correspond to angles of 26.58°, 31.89°, 39.61°, 44.18°,

and 54.85°, respectively. It was discovered that the crystallite/grain size and the lattice parameters decrease as the temperature of the deposition material rises. This size reduction would increase the crystallinity of the deposited films and increase the efficiency of photon absorption. All of the deposited materials' surface morphological images were scanned at a magnification of 200 nm. Granular nanocrystals were visible in the materials, and they were strewn unevenly and randomly throughout the glass surface. In contrast to SnS/SnO deposited at 50ºC, which has a similar image but shows the particle is scattered on the glass surface, the SnS/SnO image at room temperature shows sand-like particles well packed together without pin holes. the spectra of the absorbance demonstrate that as light radiation passed through SnS/SnO films, it absorbed radiation as the wavelength increased from the UV region to the ultraviolet region of the spectra. The absorbance also slightly decreased along the NIR infrared region as the wavelength increased. It was discovered that the precursor temperature influences the material's absorbance; as the temperature rises, the absorbance decreases, making SnS/SnO an excellent material for photovoltaic systems. The transmittance in the visible area of the spectrum was stable and SnS/SnO was at its maximum in the UV region, it increased as the wavelength increased in the NIR region. The transmittance was also impacted by temperature, which led to an increase in SnS/SnO transmittance in the UV and ultraviolet parts of the spectrum. The energy band gap spectra of the deposited SnS/SnO films were determined from the film at ambient temperature. It was found that the sample processed at room temperature had the largest energy band gap. SnS/SnO reveals an increase in thickness from 114.42– 116.54 nm which resulted in a downturn in the resistivity of the deposited film from 9.040×10^{9} – 6.455×10^{9} ($\Omega\cdot$cm) while the conductivity of the deposited material increased from 1.106×10^{-10} - 1.549×10^{-10} $(\Omega\cdot\text{cm})^{-1}$.

Acknowledgment

The research was funded by Tetfund Institution Based Research (IBR), which the authors acknowledge.

ORCID IDs

Imosobomeh L. Ikhioya, https://orcid.org/0000-0002-5959-4427

REFERENCE

[1] B. Zhao, H. Zhuang, Y. Yang, Y. Wang, H. Tao, Z. Wang, and Y. Jiang, "Composition-dependent lithium storage performances of SnS/SnO_2 heterostructures sandwiching between spherical graphene", Electrochimica Acta, **300**, 253-262 (2019). https://doi.org/10.1016/j.electacta.2019.01.116

[2] Y. Akaltun, A. Astam, A. Cerhan and T. Çayir, "Effects of thicknes on electrical properties of SILAR deposited SnS thin films", AIP Conference Proceedings, **1722**, 220001 (2016). https://doi.org/10.1063/1.4944233

[3] Z. Chen, D. Yin, and M. Zhang, "Sandwich-like MoS2@ SnO2@ C with high capacity and stability for Sodium/Potassium ion batteries", Small, **14**, 1703818 (2018). https://doi.org/10.1002/smll.201703818

[4] Y. Zheng, T. Zhou, C. Zhang, J. Mao, H. Liu, and Z. Guo, "Boosted charge transfer in SnS/SnO2 heterostructures: toward high rate capability for sodium-ion batteries", Angewandte Chemie, **128**(10), 3469-3474 (2016). https://doi.org/10.1002/ange.201510978

[5] X. Zhu, N.R. Monahan, Z. Gong, H. Zhu, K.W. Williams, and C.A. Nelson, "Charge transfer excitons at van der Waals interfaces", Journal of the American Chemical Society, **137**(26), 8313-8320 (2015). https://doi.org/10.1021/jacs.5b03141

[6] P. Zubko, S. Gariglio, M. Gabay, P. Ghosez, and J.M. Triscone, "Interface physics in complex oxide heterostructures", Annu. Rev. Condens. Matter Phys. **2**(1), 141-165 (2011). https://doi.org/10.1146/annurev-conmatphys-062910-140445

[7] C. Huang, S. Wu, A.M. Sanchez, J.J. Peters, R. Beanland, J.S. Ross, P. Rivera, W. Yao, D.H. Cobden, and X. Xu, "Lateral heterojunctions within monolayer $MoSe_2$–WSe_2 semiconductors", Nature materials, **13**(12), 1096-1101 (2014). https://doi.org/10.1038/nmat4064

[8] D.Y. Yu, P.V. Prikhodchenko, C.W. Mason, S.K. Batabyal, J. Gun, S. Sladkevich, A.G. Medvedev, and O. Lev, "High-capacity antimony sulphide nanoparticle-decorated graphene composite as anode for sodium-ion batteries", Nature communications, **4**(1), 1-7 (2013). https://doi.org/10.1038/ncomms3922

[9] C. Bommier, and X. Ji, "Recent development on anodes for Na-ion batteries", Israel Journal of Chemistry, **55**(5), 486-507 (2015). https://doi.org/10.1002/ijch.201400118

[10] H. Bian, Z. Li, X. Xiao, P. Schmuki, J. Lu, and Y.Y. Li, "Tunable transformation between SnS and SnOx nanostructures via facile anodization and their photoelectrochemical and photocatalytic performance", Solar RRL, **2**(11), 1800161 (2018). https://doi.org/10.1002/solr.201800161

[11] M. Sugiyama, Y. Murata, T. Shimizu, K. Ramya, C. Venkataiah, T. Sato, and K.R. Reddy, "Sulfurization growth of SnS thin films and experimental determination of valence band discontinuity for SnS-related solar cells", Japanese Journal of Applied Physics, **50**(5S2), 05FH03 (2011). https://doi.org/10.1143/JJAP.50.05FH03

[12] A.Y. El-Etre, and S.M. Reda, "Characterization of nanocrystalline SnO_2 thin film fabricated by electrodeposition method for dye-sensitized solar cell application", Applied Surface Science, **256**(22), 6601-6606 (2010). https://doi.org/10.1016/j.apsusc.2010.04.055

[13] B. Yuliarto, N. Nugraha, B. Epindonta, R. Aditia, and M. Iqbal, "Synthesis of SnO_2 Nanostructure Thin Film and its Prospective as Gas Sensors", Advanced Materials Research, **789**, 189–92 (2015). https://doi.org/10.4028/www.scientific.net/AMR.789.189

[14] K. Jain, R.P. Pant, and S.T. Lakshmikumar, "Effect of Ni doping on thick film SnO_2 gas sensor", Sens. Actuators B, **113**, 823 (2006). https://doi.org/10.1016/j.snb.2005.03.104

[15] Li X., Gao C., Duan H., Lu B., Wang Y., Chen L., Zhang Z., Pan X. and L.E. Xie, "High-performance photoelectrochemical - typeself powered UV photodetector using epitaxial TiO_2/SnO_2 branched heterojunction nanostructure", Small, **9**, 2005 (2013). https://doi.org/10.1002/smll.201202408

[16] W. Tian, T. Zhai, C. Zhang, S.-L. Li, X. Wang, F. Liu, D. Liu, et al, "Low-cost fully transparent ultraviolet photodetectors based on electrospun ZnO-SnO_2 heterojunction nanofibers", Adv. Mater. **25**, 4625–30 (2013). https://doi.org/10.1002/adma.201301828
[17] Q. Jiang, X. Zhang, and J. You, "SnO_2: a wonderful electron transport layer for perovskite Solar Cells", Small, **14**, 1801154 (2018). https://doi.org/10.1002/smll.201801154

СИНТЕЗ НАНОСТРУКТУРНОГО МАТЕРІАЛУ SnS/SnO ДЛЯ ФОТОЕЛЕКТРИЧНОГО ЗАСТОСУВАННЯ

Егвуньєнга Н. Джозефін[a,b], Окунзува С. Ікпонмвоса[b], Імособоме Л. Іхіоя[c]
[a]Відділ наукових лабораторних технологій, Delta State Polytechnic, Ogwashi-Uku, Нігерія
[b]Фізичний факультет, Університет Беніну, Бенін
[c]Факультет фізики та астрономії, Університет Нігерії, Нсукка, 410001, штат Енугу, Нігерія

Основні моменти дослідження:

• Успішно синтезовано наноструктурний матеріал SnS/SnO з використанням наступної техніки поглинання та реакції іонного шару (SILAR).

• У матеріалах було видно зернисті нанокристали, які були нерівномірно та хаотично розкидані по всій поверхні скла.

• Було виявлено, що зразок, оброблений при кімнатній температурі, мав найбільшу заборонену зону.

• Коефіцієнт пропускання у видимій частині спектру був стабільним, а SnS/SnO був максимальним в УФ-області

У цьому дослідженні метод SILAR використовувався для синтезу екологічно чистого матеріалу SnS/SnO для фотоелектричного застосування, де 0,1 М дигідрату хлориду олова (II) ($SnCl_2 \cdot 2H_2O$) використовувалося для створення розчину катіонного прекурсора, а 0,01 М тіоацетамід (C_2H_5NS) використовували для створення розчину аніонного прекурсора. Рентгенівські дифрактограми матеріалу SnS/SnO, нанесеного на скляну підкладку при різних температурах осадження, зафіксували основний пік при 45°C при 2 тета 31,8997°, що відповідає гранецентрованій кубічній кристалічній структурі (FCC). На картині видно дифракційні піки в площинах 111, 200, 210, 211 і 300, які відповідають кутам 26,58°, 31,89°, 39,61°, 44,18° і 54,85° відповідно. Було виявлено, що розмір кристалітів/зерен і параметри решітки зменшуються з підвищенням температури матеріалу осадження. У матеріалах було видно зернисті нанокристали, які були нерівномірно та безладно розкидані по всій поверхні скла. Спектри поглинання демонструють, що коли світлове випромінювання проходило через плівки SnS/SnO, воно поглинало випромінювання, коли довжина хвилі зростала від УФ-області до ультрафіолетової області спектру. Було виявлено, що температура прекурсора впливає на поглинання матеріалу; у міру підвищення температури абсорбція зменшується, що робить SnS/SnO чудовим матеріалом для фотоелектричних систем. Коефіцієнт пропускання у видимій області спектру був стабільним, а SnS/SnO був максимальним в УФ-діапазоні, він зростав зі збільшенням довжини хвилі в ближньому ІЧ-діапазоні. Було виявлено, що зразок, оброблений при кімнатній температурі, мав найбільшу заборонену зону. SnS/SnO виявляє збільшення товщини від 114,42 до 116,54 нм, що призвело до зниження питомого опору осадженої плівки з $9{,}040\times10^{9}$ (Ω·см) до $6{,}455\times10^{9}$ (Ω·см), тоді як провідність осадженого матеріалу зросла з $1{,}106\times10^{-10}$ $(\Omega\cdot см)^{-1}$ до $1{,}549\times10^{-10}$ $(\Omega\cdot см)^{-1}$.

Ключове слово: *сульфід олова; нанокристали, наноструктура; EDX; XRD; SEM*